Matter radius of ^{78}Kr from proton elastic scattering at 153 MeV

J. T. Zhang,[1,*] P. Ma,[1,*] Y. Huang,[1,2] X. L. Tu,[1,3,†] P. Sarriguren,[4] Z. P. Li,[5] Y. Kuang,[5] W. Horiuchi,[6,7,8,9] T. Inakura,[10] L. Xayavong,[11] Y. Sun,[12] K. Kaneko,[13] X. Q. Liu,[2] K. Yue,[1,3] C. J. Shao,[1] Q. Zeng,[14] B. Mei,[15] P. Egelhof,[16] Yu. A. Litvinov,[16] M. Wang,[1] Y. H. Zhang,[1] X. H. Zhou,[1] and Z. Y. Sun[1]

[1]*Institute of Modern Physics, Chinese Academy of Sciences, Lanzhou 730000, China*
[2]*Key Laboratory of Radiation Physics and Technology of the Ministry of Education, Institute of Nuclear Science and Technology, Sichuan University, Chengdu 610064, China*
[3]*School of Nuclear Science and Technology, University of Chinese Academy of Sciences, Beijing 100049, China*
[4]*Instituto de Estructura de la Materia, CSIC, Serrano 123, E-28006 Madrid, Spain*
[5]*School of Physical Science and Technology, Southwest University, Chongqing 400715, China*
[6]*Department of Physics, Osaka Metropolitan University, Osaka 558-8585, Japan*
[7]*Nambu Yoichiro Institute of Theoretical and Experimental Physics (NITEP), Osaka Metropolitan University, Osaka 558-8585, Japan*
[8]*RIKEN Nishina Center, Wako 351-0198, Japan*
[9]*Department of Physics, Hokkaido University, Sapporo 060-0810, Japan*
[10]*Laboratory for Zero-Carbon Energy, Institute of Innovative Research, Tokyo Institute of Technology, Tokyo 152-8550, Japan*
[11]*Department of Physics, Faculty of Natural Sciences, National University of Laos, Vientiane 01080, Laos*
[12]*School of Physics and Astronomy, Shanghai Jiao Tong University, Shanghai 200240, China*
[13]*Department of Physics, Kyushu Sangyo University, Fukuoka 813-8503, Japan*
[14]*Engineering Research Center of Nuclear Technology Application, East China University of Technology, Nanchang 330013, China*
[15]*Sino-French Institute of Nuclear Engineering and Technology, Sun Yat-sen University, Zhuhai 519082, China*
[16]*GSI Helmholtzzentrum für Schwerionenforschung GmbH, D-64291 Darmstadt, Germany*

(Received 14 May 2023; accepted 13 July 2023; published 25 July 2023)

Small-angle differential cross sections of proton elastic scattering off ^{78}Kr with a collision energy of 152.7 MeV/u were measured at the experimental Cooler Storage Ring of the Heavy Ion Research Facility in Lanzhou (HIRFL-CSR). Low energy recoil protons from the elastic scattering were counted by a silicon-strip detector to determine relative differential cross sections. A model-dependent root-mean-square matter radius of 4.16(12) fm for the ^{78}Kr nucleus was deduced by employing the Glauber model. Compared to the proton radius of 4.13 fm for ^{78}Kr, our center value of matter radius is slightly larger. This finding in ^{78}Kr is opposite to the known results of ^{76,80}Kr, where the matter radii are smaller than the corresponding proton radii. However, considering the relatively large radius error of ^{78}Kr, the difference is not statistically significant, and further experiments are necessary.

DOI: 10.1103/PhysRevC.108.014614

I. INTRODUCTION

Density-dependent nuclear symmetry energy, as a key term of the equation of state (EOS) of isospin asymmetric nuclear matter, plays an important role in nuclear physics and astrophysics investigations [1]. Many independent efforts were made to constrain the symmetry energy. However, the slope parameter L of the symmetry energy at the saturation density has still a large spread from about 20 to 120 MeV, see Refs. [2,3] and references cited therein. The precise determination of the symmetry energy is an open issue that continues attracting much attention [4]. As known, the difference of neutron distribution radius (R_n) and proton distribution radius (R_p) in a nucleus, termed the neutron skin $\Delta R_{np} = R_n - R_p > 0$, describes an excess of neutrons on the nuclear surface. It is not only an intriguing phenomenon found in neutron-rich nuclei in the last decades [5], but also an essential means for constraining L [6]. For example, a linear relationship between ΔR_{np} and L was established [6]. Although the parity violating electron scattering experiment has been developed recently [7,8], most of the ΔR_{np} measurements, especially for exotic nuclei, were model-dependent, which would result in large systematic deviations, if some effects were not considered. The compiled ΔR_{np} for ^{208}Pb span from about 0.1 to 0.3 fm [9]. A systematic deviation in the oxygen isotopes was also observed [10].

In the mass region with neutron number (N) $\approx$ proton number (Z) $\approx$36, shape coexistence and ground state shape changes were reported [11,12]. The deformations would result in changes of nucleon occupation numbers on outer orbits, thereby affecting the size of nuclei. Therefore experiments to measure matter radii [13–15] and charge radii [16] were

*These authors contributed equally to this work.
†tuxiaolin@impcas.ac.cn

pursued in this mass region. An anomalous decrease of the matter radii with increasing neutron number was experimentally observed in neutron-deficient Ga, Ge, Br, and other isotopic chains [13]. Additionally proton skin issue in ^{63}Ga was discussed in Ref. [16]. Furthermore, the proton radii of ^{76}Kr and ^{80}Kr were found to be larger than their matter radii, see Fig. 5 in Ref. [14]. This difference between proton and matter radii is similar to that found in neutron deficient nuclei such as B and Na, which have a proton skin (halo) structure [17,18]. It points to there is a possible proton skin structure ($\Delta R_{np} < 0$) in ^{76}Kr and ^{80}Kr, although the formation of a proton skin is rather difficult for nuclei with large Z due to the high Coulomb barrier [19]. If the proton skin structure in this mass region is confirmed, it would be a significant constraint for theoretical models. Along the Kr isotopic chain, the nuclear deformation of ^{76}Kr and ^{80}Kr evolve from prolate to oblate shapes. The stable nucleus ^{78}Kr lies between ^{76}Kr and ^{80}Kr, where a coexistence of prolate and oblate shapes was reported [11,20]. The matter radius determinations of ^{78}Kr by different experimental methods would provide an important milestone for understanding the difference between proton and matter radii.

Radius measurements for gaseous isotopes, such as krypton, are not easily operated in normal kinematics. In the present work, we report the matter radius measurement of ^{78}Kr via the small-angle differential cross sections of proton-nucleus elastic scatting based on inverse kinematics in a heavy-ion storage ring. The small-angle differential cross sections of proton scattering off nuclei are from the peripheral collisions, which are sensitive to matter radii of nuclei related to surface density distributions.

II. EXPERIMENT

The in-ring reaction experiment was conducted at the Cooler Storage Ring of the Heavy Ion Research Facility in Lanzhou (HIRFL-CSR) [21], see Fig. 1. Such kinds of experiments were characterized by windowless target, low momentum detection sensitivity, and low background [22–28]. The feasibility experiment at the HIRFL-CSR has been carried out with ^{58}Ni$(p,\ p)^{58}$Ni reaction [24]. In the present work, the $^{78}Kr^{26+}$ beam with an energy of 5.9 MeV/u from the sector focusing cyclotron (SFC) was accelerated to an energy of 152.7 MeV/u in the main storage ring (CSRm). Afterwards, the beam was fast extracted from the CSRm, transported through the projectile fragment separator (RIBLL2), and injected into the experimental storage ring (CSRe). The CSRe was operated for an internal target experiment at a mean magnetic rigidity of about 5.545 Tm. A vacuum of about 10^{-11} mbar was maintained in the CSRe, enabling the $^{78}Kr^{26+}$ to be stored for a sufficiently long time. The stored ^{78}Kr ions in the CSRe interacted repeatedly with the hydrogen target, which was generated by the internal gas-jet target system of the CSRe [29]. The molecular hydrogen-gas target has a typical diameter of about 4 mm and a thickness of about 10^{12} atoms/cm^2 [29]. The energy loss of the ions due to collisions with the target and residual gas was compensated by the electron cooling [30].

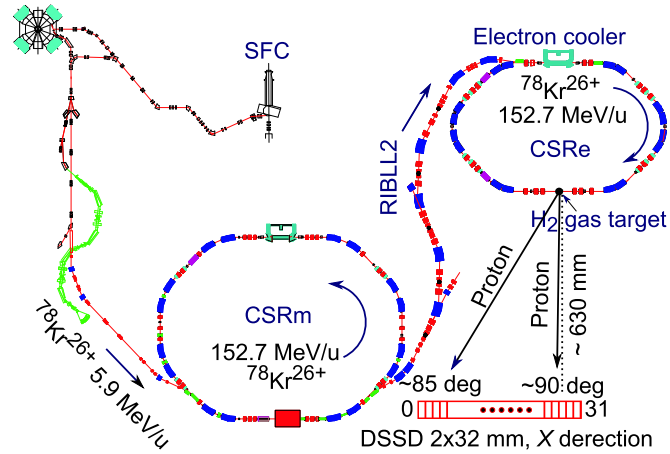

FIG. 1. Schematic illustration of the setup for the in-ring ^{78}Kr$(p,\ p)^{78}$Kr experiment.

In our context, the size and the thickness of the gas target are, respectively, very small and thin [29], such that the flight paths and energies of recoil protons from elastic scattering would not be changed by secondary collisions with the gas target. As a result, the differential cross sections of proton elastic scattering can be precisely determined by measuring the number of recoiling protons as a function of their energies. A MICRON double-sided Si-strip detector (DSSD) BB7 with a thickness of 1000 μm was installed for measuring the low energy recoil protons around 90° and at a distance of about 630 mm from the collision point, see Fig. 1. The DSSD was fully compatible with the ultra-high vacuum environment and has an active area of 64×64 mm^2. It was segmented into 32×32 strips in X and Y directions. The strip width is 1.96 mm. The DSSD covers the laboratory angular range from about 85° to 90° in the X direction. The energies of elastic recoil protons depend on scattering angles. The Mesytec MPR-16 preamplifier and the MSCF-16 shaping amplifier were used to process the signals from the DSSD. All signals were recorded by a data acquisition system (DAQ), which was triggered by a logic OR signal. In order to reduce the effects of noise, an energy threshold of about 400 keV was set for the trigger in this experiment. As shown in Fig. 2, the energy of each strip was calibrated by β and α particles with energies of 0.482 MeV, 0.554 MeV, 0.976 MeV, 1.048 MeV, 5.388 MeV, 5.443 MeV, and 5.486 MeV from ^{207}Bi and ^{241}Am radioactive sources, respectively. The obtained energy resolutions, $\Delta E/E$(FWHM), were about 2.6%, 1.1%, and 0.4% at energies of about 0.5 MeV, 1 MeV, and 5.5 MeV, respectively. Otherwise, the detection efficiency also plays an important role in extracting differential cross sections. In the present work, the detection efficiencies at different energies were measured by using α particles from the ^{241}Am source. The different energies of α particles were obtained by changing gas pressure in vacuum chamber. As shown in the insert of Fig. 2, there is no obvious difference for the relative detection efficiency in the energy range from about 0.5 to 5.5 MeV.

Figure 3 shows the measured recoil proton energies of ^{78}Kr$(p,\ p)^{78}$Kr reaction as a function of the strip number of

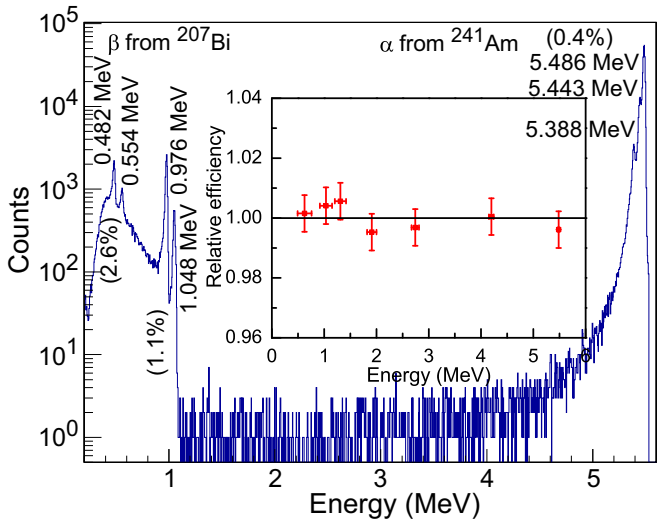

FIG. 2. A typical calibration energy spectrum from ^{207}Bi and ^{241}Am radioactive sources. The values in parenthesis are energy resolutions. The insert shows the relative detection efficiency measured by α particles with different energies. The horizontal error bars on the data indicate the energy spread (FWHM), which was caused by the energy loss of α particles in gas.

the DSSD. The energy dispersion in each strip was mainly caused by the strip width and target distribution. Compared to the calculations by the relativistic kinematics [31,32], a precision of about 0.4% was achieved for the average proton energies measured by Si strips, see Fig. 3. More details on the in-ring reaction experimental setup can be found in Ref. [25].

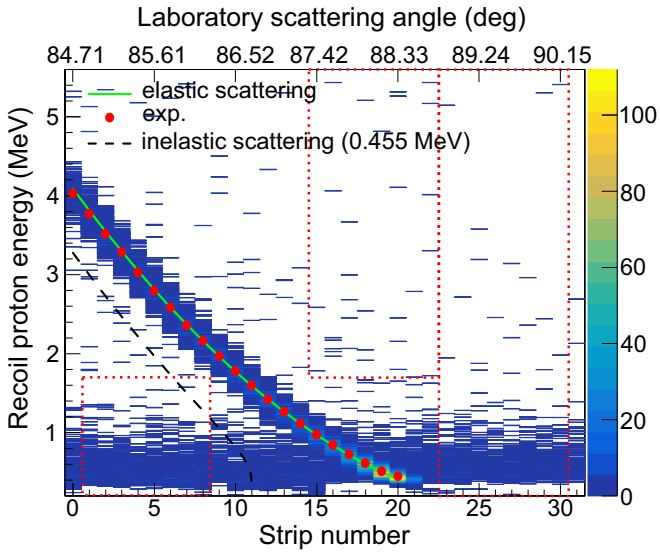

FIG. 3. Measured energies of recoil protons as a function of the strip number in the X direction. The events in the rectangles enclosed by red dotted curves were taken as samples to calculate the total background. The green solid and black dashed lines denote the calculated recoil proton energies for elastic scattering and inelastic scattering with an excitation energy of 0.455 MeV [20], respectively. The filled red circles are the measured average energies of the elastically scattered protons.

III. DATA ANALYSIS

Precise measurement of reaction luminosity is a challenging task for the in-ring reaction experiments, since it is difficult to precisely determine gas-target density, beam intensity, and the overlap between the target and the beam [33]. To reduce the error bars caused by the uncertainty of absolute normalization, the matter radius of ^{78}Kr was deduced through relative differential cross sections. A similar method has been used to determine matter radii of ^{20,22}Ne, ^{24,26}Mg [34], and ^{16}O [35] in the previous work. To further check the possible uncertainties caused by the relative analysis, we inspected data from Ref. [36] to extract the matter radius of ^{12}C based on the symmetrized Fermi (SF) distribution model, where the matter and proton radii of ^{12}C are expected to be almost the same. The obtained radius of 2.35(2) fm for ^{12}C agrees very well with the result based on the SF density model in Ref. [36]. It indicates the employed method does not introduce extra error into resultant radius.

A. Relative differential cross sections

The elastic scattering angles have a one-to-one relationship with the measured proton kinetic energies. The relative differential cross sections $\frac{d\sigma}{d\Omega}(\theta)_{re}$ can be obtained using the relations [31,32]

$$2m_pK_{\rm lab} = 2p^2(1-\cos\theta),$$
$$\frac{d\sigma}{d\Omega}(\theta)_{re} = \frac{1}{\sin\theta}\left(\frac{\Delta N_{\rm all}}{\Delta\theta} - \frac{\Delta N_{bg}}{\Delta\theta}\right), \quad (1)$$

where m_p, $K_{\rm lab}$, and p are the rest proton mass, measured proton kinetic energy, and momentum in the center-of-mass frame, respectively. $\Delta N_{\rm all}$ and ΔN_{bg} are the numbers of measured total events and background events in the bin size $\Delta\theta$ of the scattering angle θ in the center-of-mass frame, respectively. In this experiment, p was 550.5 MeV. We can see that the angular resolutions of differential cross sections are mainly influenced by the energy resolutions of the DSSD, because the flight paths and energies of protons would not be affected by the gas target. The used $\Delta\theta$ of 0.1° corresponds to an energy difference of about 4%, which is larger than the measured energy resolution, see Fig. 2.

As shown in Fig. 3, the inelastic scattering events from the state with an excitation energy of 0.455 MeV [20] can clearly be distinguished. The measured energies of the elastically scattered protons are in the range from about 0.4 to 4.5 MeV. Thus, the DSSD used in this work was thick enough to effectively stop the scattered protons. To reduce the effects of the gas target distribution and the geometry of the vacuum chamber on solid angle, according to the GEANT4 simulations, only events with energies in the range from about 0.5 to 3 MeV were considered in the analysis, which corresponds to scattering angles θ from about 3.25° to 7.75°, see Fig. 4. In particular, the detection efficiencies in this energy range were about consistent, see the insert in Fig. 2. We note that there is a difference of about 0.3% for the azimuth angles

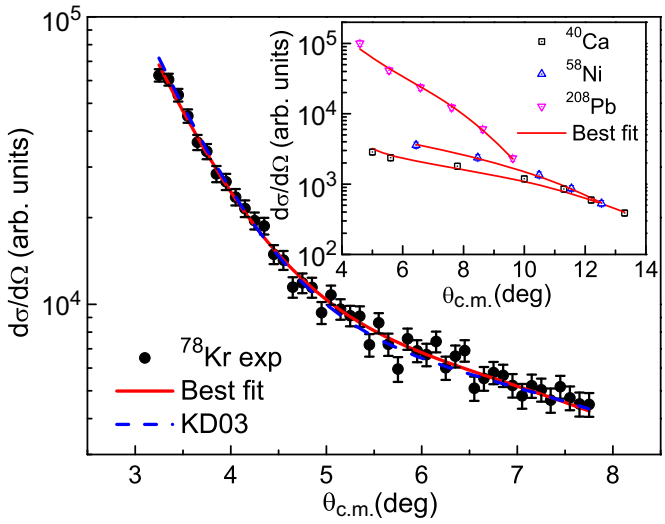

FIG. 4. The best fit of the $\frac{d\sigma}{d\Omega}(\theta)_{re}$ for ^{78}Kr as a function of θ in the center-of-mass frame (red solid line). The blue dashed line indicates the calculated differential cross sections by using the FRESCO program [38] with the phenomenological OMP parameters (KD03) [37]. The insert shows the best fit of the small-angle relative differential cross sections for ^{40}Ca, ^{58}Ni, and ^{208}Pb [58–60]. Relative differential cross sections $\frac{d\sigma}{d\Omega}(\theta)_{re}$ were normalized to the calculated absolute cross sections of the Glauber model by multiplying with A_0.

ϕ covered by an individual strip. However, compared to a statistical fluctuation of about 9% for the relative differential cross sections, these small uncertainties were neglected in the present analysis. The background contributions are mainly from cosmic rays, scattered residual gas particles, and electronic noises. To reduce the background of electronic noises, only the coincident events between the X and Y strips were considered. The measured background events from 16 strips in the rectangles enclosed by red dotted curves, see Fig. 3, were used to estimate the total background of 32 strips. The obtained background counts were subtracted from total counts according to formula 1. Multiple events were attributed as cross-talk signals and thus excluded in our analysis.

Figure 4 shows the obtained relative differential cross sections of ^{78}Kr(p, p)^{78}Kr in this work. As known, the phenomenological optical model potentials (OMP) describe well the differential cross sections of proton elastic scattering. The global phenomenological OMP (KD03) parameters were extracted through proton elastic scattering data with incident energies from 1 keV up to 200 MeV [37]. The reaction cross sections for proton scattering on stable nuclei can be reproduced with a precision of 5% to 10% by the KD03 parameters. As shown in Fig. 4, the trend of our differential cross sections is as well consistent with the calculated result by using the KD03 parameters [37] based on the FRESCO program [38]. It indicates a reliability of our differential cross sections.

B. Extraction of the matter radius

Proton-nucleus elastic scattering can provide direct information on matter density distribution of a nucleus through appropriate reaction models. The matter radius of ^{78}Kr was extracted by fitting the measured small-angle $\frac{d\sigma}{d\Omega}(\theta)_{re}$ with a procedure based on the Glauber model [39]. This reaction model has been widely adopted to extract matter radii of nuclei, see Refs. [36,40–43] and references cited therein. Basic formulas used for the analysis of proton-nucleus elastic scattering in this work are similar to those used for the analysis of the IKAR data [43]. The differential cross sections of proton-nucleus elastic scattering were calculated in the Glauber model via [43]

$$\frac{d\sigma}{d\Omega}(\theta) = |F_{el}(\boldsymbol{q})|^2, \tag{2}$$

where the elastic scattering amplitude $F_{el}(\boldsymbol{q})$ is a function of matter density $\rho(r)$ and nucleon-proton profile function γ_{Np}. The γ_{Np} is related to the free nucleon-proton scattering amplitude f_{Np} as

$$f_{Np} = \frac{ik}{4\pi}\sigma_{Np}(1 - i\alpha_{Np})\exp\left(-\frac{\boldsymbol{q}^2\beta_{Np}}{2}\right), \tag{3}$$

where σ, α, and β are the total cross sections, ratios of the real to imaginary parts of the forward-scattering amplitudes, and slope parameters, respectively. The index Np represents proton-proton (pp) and neutron-proton (np) channels.

Similar to the radius extractions of ^{76}Kr and ^{80}Kr [14], the matter density distribution was described by the two-parameter Fermi (2pF) model in this work,

$$\rho(r) = \rho(0)\frac{1}{1 + \exp\left(\frac{r-R}{a}\right)}, \tag{4}$$

where $\rho(0)$ is the density normalization factor. R and a are the half-density radius and the diffuseness parameter, respectively. Our differential cross sections in this angle region cannot constrain R and a simultaneously [22,44], since the first diffraction minimum was not covered [22]. As known, the reported a of the charge densities and folded matter densities for the stable medium-heavy nuclei are almost constant, and are in the range from 0.5 to 0.6 fm [41,45]. Thus, as the used method in Refs. [14,17,46], the diffuseness parameter a was fixed to be 0.55(3) fm in this work, which was determined by the matter density distributions of neighboring ^{58}Ni and ^{90}Zr nuclei [47]. The uncertainty of the diffuseness parameter only results in a difference of about 0.02 fm for matter radius.

In the χ^2-minimization procedure for ^{78}Kr, the half-density radius R and the absolute normalization A_0 were used as free parameters to fit the obtained relative differential cross sections. The χ^2 function is defined as

$$\chi^2 = \sum_j^{N_0} \frac{\left[A_0\frac{d\sigma}{d\Omega}(\theta_j)_{re} - \frac{d\sigma}{d\Omega}(\theta_j)_{\rm cal}\right]^2}{\left[A_0\Delta\frac{d\sigma}{d\Omega}(\theta_j)_{re}\right]^2}, \tag{5}$$

where N_0 and $\Delta\frac{d\sigma}{d\Omega}(\theta)_{re}$ are the number of data points and the uncertainties of relative differential cross sections, respectively. $\frac{d\sigma}{d\Omega}(\theta)_{\rm cal}$ are the differential cross sections calculated with the Glauber model. Subsequently, the matter radius R_m was calculated by taking the obtained R and fixed a via

$$R_m = \left(\frac{\int \rho(r)r^4dr}{\int \rho(r)r^2dr}\right)^{\frac{1}{2}}. \tag{6}$$

TABLE I. The Np scattering amplitudes used in the Glauber model calculations. The matter radii R_m are the results from this work. R_m^{lit} as radii of reference were deduced from the compiled neutron skin thicknesses [9] and proton radii. The errors of R_m^{lit} are only statistical uncertainties. The $\beta_{pp} = \beta_{np} = 0.68(3)\,\mathrm{fm}^2$ was adopted to reproduce the matter radii of ^{40}Ca, ^{58}Ni, and ^{208}Pb based on the 2pF density model, where a was fixed to be 0.55 fm, see text.

Nuclei	E_p MeV	$\sigma_{pp}^{\mathrm{corr}}$ mb	$\sigma_{Np}^{\mathrm{corr}}$ mb	α_{pp}	α_{np}	R_m^{lit} fm	R_m fm
^{78}Kr	153.8	16.60(27)	33.70(42)	1.507(20)	0.883(14)		4.16(12)
^{40}Ca	156.0	16.68	33.55	1.486	0.871	3.39(1)	3.40
^{58}Ni	160.0	16.82	33.28	1.454	0.853	3.69(1)	3.68
^{208}Pb	160.0	16.82	33.28	1.454	0.853	5.55(1)	5.56

At intermediate and high energies, the free Np scattering amplitudes can directly be used to analyze the data [36,43]. However, due to Pauli blocking, in-medium modifications of σ have to be considered at low and intermediate energies [48]. The in-medium total cross sections $\sigma_{Np}^{\mathrm{corr}}$ for nucleon-nucleus scattering were estimated via [48]

$$\sigma_{Np}^{\mathrm{corr}} = \sigma_{Np}^{\mathrm{free}}\left(1 - \frac{7}{5}\frac{E_f}{E_p}\right), \tag{7}$$

where $\sigma_{Np}^{\mathrm{free}}$ and E_p are the free Np scattering total cross section and the kinetic energy of proton beam, respectively. The Fermi energy is $E_f = (3\pi^2\rho/2)^{\frac{2}{3}}\hbar^2/2m_N = 36.87(89)$ MeV, where the normal nuclear density $\rho\,0.160(6)\,\mathrm{nucleons/fm}^3$ was chosen [49].

In the present analysis, $\sigma_{Np}^{\mathrm{free}}$ were determined by fitting the experimental data compiled by the Particle Data Group [50] with the formulas from Ref. [51]. To improve precision, the used α_{Np} were obtained by averaging data from Refs. [50–57]. To reduce model uncertainty, as described in Ref. [43], the $\beta_{pp} = \beta_{np}$ was calibrated by fitting the small-angle relative differential cross sections of proton scattering on ^{40}Ca [58], ^{58}Ni [59], and ^{208}Pb [59] at 156 MeV and 160 MeV to reproduce their matter radii, see the insert in Fig. 4. These differential cross sections are available in EXFOR [60]. Model-independent radii data would be an ideal calibrating reference. However, we noted that the results of ^{208}Pb [7] and ^{48}Ca [8] determined by the model-independent parity violation electron scattering are not very consistent. As a result, the compiled neutron skin thicknesses from different experimental methods [9] were used to deduce reference matter radii of ^{40}Ca, ^{58}Ni, and ^{208}Pb, see Table I. The obtained value of $0.68(3)\,\mathrm{fm}^2$ for the $\beta_{pp} = \beta_{np}$ can reproduce the matter radii of ^{40}Ca, ^{58}Ni, and ^{208}Pb within about 0.01 fm, see Table I. This obtained value slightly deviates from the β of $0.58\,\mathrm{fm}^2$ in Ref. [52], which would result in a matter radius difference of about 0.02 fm for ^{78}Kr. The Np amplitudes and matter radii are summarized in Table I.

Figure 4 shows the best fit with χ^2/N_0 of about 37/46 for the relative differential cross sections as a function of scattering angle in the center-of-mass frame. The deduced model-dependent root-mean-square (rms) point-matter radius for ^{78}Kr is 4.16(12) fm. As shown in Fig. 3, the background is mainly distributed in the region of energies <0.8 MeV, which corresponds to a scattering angle of about 4.05°. To check the effects of background, we also fitted the relative differential cross sections in the range from 4.05° to 7.75°, and a consistent radius of 4.15 fm was obtained.

The statistical error of matter radius is about 0.10 fm, which is a standard deviation of matter radii determined through randomly sampling experimental $\frac{d\sigma}{d\Omega}(\theta)_{re}$ within a confidence level of 95.4% based on Gaussian distribution. The uncertainties of the used input parameters cause a radius error of about 0.07 fm. Otherwise, there would be a model error of about 0.02 fm, if we used the method in Ref. [17] that fixed the half-density radius R, and then adjusted the diffuseness parameter a. In general, uncertainties, such as due to input parameters and density distribution model, can be eliminated by calibrating β to reproduce matter radii. Thus, it would be useful to calibrate β by measuring under the same experimental conditions the small-angle differential cross sections of proton elastic scattering on neighboring nuclei with well-known radii.

IV. DISCUSSION

The relation between the point-proton distribution radius R_p and charge radius R_{ch} includes various corrections [61]. Among them, Darwin-Foldy and spin-orbit terms are quite small. The most important correction comes from the finite size effects of the proton and neutron. Consequently, R_p of about 4.13 fm for ^{78}Kr was calculated using R_{ch} [62] via $R_p^2 = R_{ch}^2 - r_p^2 - \frac{N}{Z}r_n^2$. The charge radius of the proton r_p and the squared charge radius of the neutron r_n^2 are 0.8783 fm and $-0.1149\,\mathrm{fm}^2$ [62], respectively. Compared to the proton radius of ^{78}Kr, our center value of the matter radius is slightly larger. The point-neutron distribution radius R_n of 4.19(22) fm for ^{78}Kr can be obtained by using our matter radius via $R_n^2 = \frac{A}{N}R_m^2 - \frac{Z}{N}R_p^2$, which is consistent with R_p within uncertainties. And then a $\Delta R_{np} = R_n - R_p = 0.06(22)$ fm for ^{78}Kr was determined in this work. Our center value of ΔR_{np} agrees with a neutron skin thickness of 0.038(32) fm, which was calculated via an empirical linear relationship deduced from the antiprotonic atom x-ray experiments, namely, $\Delta R_{np} = (-0.04 \pm 0.03) + (1.01 \pm 0.15)(N-Z)/A$ [63]. Our ΔR_{np} seems to indicate that there exists no obvious proton skin structure. However, the proton radii of ^{76}Kr and ^{80}Kr were found to be larger than the matter radii, see Fig. 5 in Ref. [14]. This difference would not be able to understand through deformation. If taken the matter radii of ^{76}Kr and ^{80}Kr from Ref. [14], ΔR_{np} of $-0.24(8)$ fm and $-0.17(8)$ fm were obtained for ^{76}Kr and ^{80}Kr combined with the proton radii

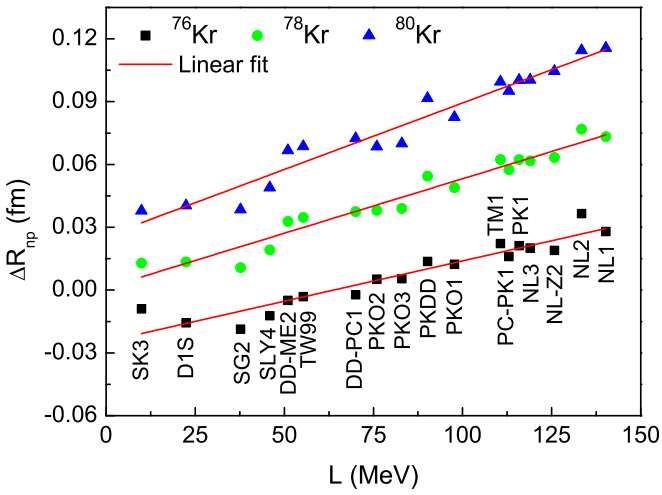

FIG. 5. Neutron skin thickness ΔR_{np} as a function of the slope L obtained by different effective interactions [67–82].

deduced from the charge radii [62], respectively. It may indicate the proton skin structure in ^{76}Kr and ^{80}Kr.

Due to the relatively large uncertainty, our result cannot effectively constrain proton or neutron skin structure in ^{78}Kr. To further study the difference between proton and matter radii for ^{76,78,80}Kr, a well-established tool from various effective interactions [6], namely, a linear relationship of the neutron skin thicknesses and the slope parameter L of symmetry energy, were adopted to analyze probability of proton or neutron skin structure. Figure 5 shows the ΔR_{np} of ^{76,78,80}Kr obtained by the nonrelativistic and relativistic models [64–66] based on various effective interactions [67–82]. These interactions cover the large spread range of L from about 10 to 140 MeV [2,3]. All calculated ΔR_{np} are positive for ^{78}Kr, see Fig. 5.

Furthermore, the deformation of the Kr isotopes may cause a change of occupation numbers, thus, result in different ΔR_{np}. Besides the above self-consistent mean-field calculations, to investigate the effect of occupation numbers on ΔR_{np}, we incorporated the shell-model occupation numbers calculated by the JUN45 Hamiltonian [83] into the realistic radial wave functions from the Woods-Saxon potential [84], which were determined by reproducing the experimental separation energies and charge radii. As a result, ΔR_{np} of 0.04 fm, 0.11 fm, and 0.17 fm were obtained by considering the occupation numbers of nucleons in ^{76}Kr, ^{78}Kr, and ^{80}Kr, respectively. Both the self-consistent mean-field and the shell-model calculations do not support the large proton skin thickness of about -0.2 fm for ^{76}Kr and ^{80}Kr. In this mass region, according to the systematic behavior of the charge radii, the authors in Ref. [16] also concluded that the existence of a proton skin in ^{63}Ga would be impossible.

As known, matter radii are approximately proportional to total reaction cross sections $\sigma_R = \sigma_I + \sigma_{\rm inel}$, where σ_I and $\sigma_{\rm inel}$ are the interaction cross sections and the inelastic cross sections, respectively. In data analyses on ^{76}Kr and ^{80}Kr, assuming $\sigma_I = \sigma_R$, the $\sigma_{\rm inel}$ was ignored [14]. However, different theories indicated that $\sigma_{\rm inel}$ could have about a few percent effect on σ_R [85,86]. We evaluated theoretical σ_R of ^{76,78,80}Kr on a carbon target with the Glauber model [39], see Refs. [86,87] for details. The input density distributions were generated by an axially symmetric Hartree-Fock-Bogoliubov method using the HFBTHO code [88]. The SkM* interaction [89] with the standard mixed-type pairing interaction was employed. The resulting matter radius of ^{78}Kr is 4.17 fm, which reproduces fairly well the experimental matter radius deduced in this work. Compared to the experimental σ_I of ^{76}Kr and ^{80}Kr [14], the theoretical σ_R values are larger by about 70 mb. If this deviation is adjusted, the matter radii of ^{76}Kr and ^{80}Kr [14] would be larger by about 0.1 fm, and the issue of the large proton skin would disappear. To further understand the difference between matter and proton radii in the $N \approx Z \approx 36$ mass region, more precise matter radii determined by different experimental methods are needed.

V. SUMMARY

The small-angle differential cross section of proton elastic scattering on ^{78}Kr was measured in inverse kinematics at the HIRFL-CSR utilizing an internal gas target. The Glauber model was used to extract matter radius through fitting the obtained relative differential cross sections. A point-matter radius of 4.16(12) fm for ^{78}Kr has been determined for the first time based on the two-parameter Fermi density model. Compared to the proton radius of ^{78}Kr, our matter radius seems slightly larger. This is different from the observed phenomena in literature, namely, that the proton radii of ^{76}Kr and ^{80}Kr are larger than their matter radii. More precise matter radii will be helpful to further understand the evolution of matter radii in the $N \approx Z \approx 36$ mass region. If the matter radii of ^{76}Kr and ^{80}Kr are confirmed, theoretical models would face major challenges to reproduce the large proton skin thickness. It would have a significant influence on the parameters of the equation of state (EOS) of isospin asymmetric nuclear matter.

ACKNOWLEDGMENTS

We would like to thank the HIRFL accelerator group for the stable beam and T. Yamaguchi for the useful discussions. This work is supported in part by the NSFC (12022504, 12121005, U1932140), by the CAS Pioneer Hundred Talents Program, and by the CAS Open Research Project of large research infrastructures. P. S. acknowledges MCI/AEI/FEDER, UE (Spain) under Grant No. PGC2018-093636-B-I00. J. T. Zhang and P. Ma contributed equally to this work and should both be considered as first authors.

[1] B. A. Li, L. W. Chen, and C. M. Ko, Phys. Rep. **464**, 113 (2008).

[2] A. Carbone, G. Colò, A. Bracco, L. G. Cao, P. F. Bortignon, F. Camera, and O. Wieland, Phys. Rev. C **81**, 041301(R) (2010).

[3] M. B. Tsang, J. R. Stone, F. Camera, P. Danielewicz, S. Gandolfi, K. Hebeler, C. J. Horowitz, Jenny Lee, W. G. Lynch, Z. Kohley *et al.*, Phys. Rev. C **86**, 015803 (2012).

[4] M. Baldo and G. F. Burgio, Prog. Part. Nucl. Phys. **91**, 203 (2016).

[5] I. Tanihata, H. Hamagaki, O. Hashimoto, Y. Shida, N. Yoshikawa, K. Sugimoto, O. Yamakawa, T. Kobayashi, and N. Takahashi, Phys. Rev. Lett. **55**, 2676 (1985).

[6] B. A. Brown, Phys. Rev. Lett. **85**, 5296 (2000).

[7] D. Adhikari, H. Albataineh, D. Androic, K. Aniol, D. S. Armstrong, T. Averett, C. Ayerbe Gayoso, S. Barcus, V. Bellini, R. S. Beminiwattha *et al.*, Phys. Rev. Lett. **126**, 172502 (2021).

[8] D. Adhikari, H. Albataineh, D. Androic, K. A. Aniol, D. S. Armstrong, T. Averett, C. Ayerbe Gayoso, S. K. Barcus, V. Bellini, R. S. Beminiwattha *et al.*, Phys. Rev. Lett. **129**, 042501 (2022).

[9] J. T. Zhang, X. L. Tu, P. Sarriguren, K. Yue, Q. Zeng, Z. Y. Sun, M. Wang, Y. H. Zhang, X. H. Zhou, and Yu. A. Litvinov, Phys. Rev. C **104**, 034303 (2021).

[10] V. Lapoux, V. Somà, C. Barbieri, H. Hergert, J. D. Holt, and S. R. Stroberg, Phys. Rev. Lett. **117**, 052501 (2016).

[11] F. Becker, A. Petrovici, J. Iwanicki, N. Amzal, W. Korten, K. Hauschild, A. Hurstel, Ch. Theisen, P. A. Butler, R. A. Cunningham *et al.*, Nucl. Phys. A **770**, 107 (2006).

[12] Y. Fu, H. Mei, J. Xiang, Z. P. Li, J. M. Yao, and J. Meng, Phys. Rev. C **87**, 054305 (2013).

[13] G. F. Lima, A. Lépine-Szily, A. C. C. Villari, W. Mittig, R. Lichtenthäler, M. Chartier, N. A. Orr, J. C. Angélique, G. Audi, E. Baldini-Neto *et al.*, Nucl. Phys. A **735**, 303 (2004).

[14] T. Yamaguchi, T. Suzuki, T. Ohnishi, F. Becker, M. Fukuda, H. Geissel, M. Hosoi, R. Janik, K. Kimura, T. Kuboki *et al.*, Phys. Rev. C **77**, 034315 (2008).

[15] A. Lépine-Szily, G. F. Lima, A. C. C. Villar, W. Mittig, R. Lichtenthäler, M. Chartier, N. A. Orr, J. C. Angélique, G. Audi, J. M. Casandjian *et al.*, Eur. Phys. J. A **25**, 227 (2005).

[16] T. J. Procter, J. Billowes, M. L. Bissell, K. Blaum, F. C. Charlwood, B. Cheal, K. T. Flanagan, D. H. Forest, S. Fritzsche, Ch. Geppert *et al.*, Phys. Rev. C **86**, 034329 (2012).

[17] T. Suzuki, H. Geissel, O. Bochkarev, L. Chulkov, M. Golovkov, D. Hirata, H. Irnich, Z. Janas, H. Keller, T. Kobayashi *et al.*, Phys. Rev. Lett. **75**, 3241 (1995).

[18] G. A. Korolev, A. V. Dobrovolsky, A. G. Inglessi, G. D. Alkhazov, P. Egelhof, A. Estradé, I. Dillmann, F. Farinon, H. Geissel, S. Ilieva *et al.*, Phys. Lett. B **780**, 200 (2018).

[19] N. Fukunishi, T. Otsuka, and I. Tanihata, Phys. Rev. C **48**, 1648 (1993).

[20] H. Sun, J. Döring, G. D. Johns, R. A. Kaye, G. Z. Solomon, S. L. Tabor, M. Devlin, D. R. LaFosse, F. Lerma, D. G. Sarantites *et al.*, Phys. Rev. C **59**, 655 (1999).

[21] J. W. Xia, W. L. Zhan, B. W. Wei, Y. J. Yuan, M. T. Song, W. Z. Zhang, X. D. Yang, P. Yuan, D. Q. Gao, H. W. Zhao *et al.*, Nucl. Instrum. Methods Phys. Res. A **488**, 11 (2002).

[22] M. von Schmid, T. Aumann, S. Bagchi, S. Bönig, M. Csatlós, I. Dillmann, C. Dimopoulou, P. Egelhof, V. Eremin, T. Furuno *et al.*, Eur. Phys. J. A **59**, 83 (2023).

[23] P. Egelhof (EXL Collaboration), JPS Conf. Proc. **35**, 011002 (2021).

[24] K. Yue, J. T. Zhang, X. L. Tu, C. J. Shao, H. X. Li, P. Ma, B. Mei, X. C. Chen, Y. Y. Yang, X. Q. Liu *et al.*, Phys. Rev. C **100**, 054609 (2019).

[25] J. T. Zhang, K. Yue, H. X. Li, X. L. Tu, C. J. Shao, P. Ma, B. Mei, X. C. Chen, Y. Y. Yang, X. Q. Liu *et al.*, Nucl. Instrum. Methods Phys. Res. A **948**, 162848 (2019).

[26] J. C. Zamora, T. Aumann, S. Bagchi, S. Bönig, M. Csatlós, I. Dillmann, C. Dimopoulou, P. Egelhof, V. Eremin, T. Furuno *et al.*, Phys. Rev. C **96**, 034617 (2017).

[27] X. Liu, P. Egelhof, O. Kiselev, and M. Mutterer, Phys. Lett. B **809**, 135776 (2020).

[28] M. Steck and Y. A. Litvinov, Prog. Part. Nucl. Phys. **115**, 103811 (2020).

[29] C. J. Shao, R. C. Lu, X. H. Cai, D. Y. Yu, F. F. Ruan, Y. L. Xue, J. M. Zhang, D. K. Torpokov, and D. Nikolenko, Nucl. Instrum. Methods Phys. Res. B **317**, 617 (2013).

[30] L. J. Mao, H. Zhao, X. D. Yang, J. Li, J. C. Yang, Y. J. Yuan, V. V. Parkhomchuk, V. B. Reva, X. M. Ma, T. L. Yan *et al.*, Nucl. Instrum. Methods Phys. Res. A **808**, 29 (2016).

[31] J. W. Norbury and F. Dick, NASA Technical Report Server No. 215543 (2008).

[32] R. L. Workman, V. D. Burkert, V. Crede, E. Klempt, U. Thoma, L. Tiator, K. Agashe, G. Aielli, B. C. Allanach, C. Amsler *et al.*, Prog. Theor. Exp. Phys. **2022**, 083C01 (2022).

[33] J. Eichler and Th. Stöhlker, Phys. Rep. **439**, 1 (2007).

[34] Z. H. Li, Y. Kuang, Y. Huang, X. L. Tu, Z. P. Li, K. H. Fang, J. T. Zhang, and K. Yue, Phys. Rev. C **107**, 064310 (2023).

[35] Y. Huang, J. T. Zhang, Y. Kuang, J. Geng, X. L. Tu, K. Yue, W. H. Long, and Z. P. Li, Eur. Phys. J. A **59**, 4 (2023).

[36] A. V. Dobrovolsky, G. A. Korolev, S. Tang, G. D. Alkhazov, G. Colò, I. Dillmann, P. Egelhof, A. Estradé, F. Farinon, H. Geissel *et al.*, Nucl. Phys. A **1008**, 122154 (2021).

[37] A. J. Koning and J. P. Delaroche, Nucl. Phys. A **713**, 231 (2003).

[38] I. J. Thompson, Comput. Phys. Rep. **7**, 167 (1988).

[39] R. J. Glauber, in *Lectures in Theoretical Physics*, edited by W. E. Brittin and L. G. Dunham (Interscience, New York, 1959), Vol. 1, p. 315.

[40] G. D. Alkhazov, S. L. Belostotsky, and A. A. Vorobyov, Phys. Rep. **42**, 89 (1978).

[41] G. D. Alkhazov, S. L. Belostotsky, O. A. Domchenkov, Yu. V. Dotsenko, N. P. Kuropatkin, V. N. Nikulin, M. A. Shuvaev, and A. A. Vorobyov, Nucl. Phys. A **381**, 430 (1982).

[42] G. D. Alkhazov, M. N. Andronenko, A. V. Dobrovolsky, P. Egelhof, G. E. Gavrilov, H. Geissel, H. Irnich, A. V. Khanzadeev, G. A. Korolev, A. A. Lobodenko *et al.*, Phys. Rev. Lett. **78**, 2313 (1997).

[43] G. D. Alkhazov, A. V. Dobrovolsky, P. Egelhof, H. Geissel, H. Irnich, A. V. Khanzadeev, G. A. Korolev, A. A. Lobodenko, G. Münzenberg, M. Mutterer *et al.*, Nucl. Phys. A **712**, 269 (2002).

[44] S. Hatakeyama, W. Horiuchi, and A. Kohama, Phys. Rev. C **97**, 054607 (2018).

[45] H. De Vries, C. W. de jager, and C. de Vries, At. Data Nucl. Data Tables **36**, 495 (1987).

[46] A. Ozawa, T. Baumann, L. Chulkov, D. Cortina, U. Datta, J. Fernandez, H. Geissel, F. Hammache, K. Itahashi, M. Ivanov *et al.*, Nucl. Phys. A **709**, 60 (2002).

[47] Y. Huang *et al.*, (unpublished).

[48] M. S. Hussein, R. A. Rego, and C. A. Bertulani, Phys. Rep. **201**, 279 (1991).

[49] L. Satpathy, V. S. Uma Maheswari, and R. C. Nayak, Phys. Rep. **319**, 85 (1999).

[50] P. A. Zyla, R. M. Barnett, J. Beringer, O. Dahl, D. A. Dwyer, D. E. Groom, C. J. Lin, K. S. Lugovsky, E. Pianori, D. J. Robinson *et al.* (Particle Data Group), Prog. Theor. Exp. Phys. **2020**, 083C01 (2020).
[51] A. Mehndiratta and P. Shukla, Nucl. Phys. A **961**, 22 (2017).
[52] L. Ray, Phys. Rev. C **20**, 1857 (1979).
[53] B. Abu-Ibrahim, W. Horiuchi, A. Kohama, and Y. Suzuki, Phys. Rev. C **77**, 034607 (2008).
[54] J. Bystricky, C. Lechanoine-Leluc, and F. Lehar, J. Phys. France **48**, 199 (1987).
[55] G. J. Igo, Rev. Mod. Phys. **50**, 523 (1978).
[56] I. Ahmad, M. A. Abdulmomen, and L. A. Al-Khattabi, Int. J. Mod. Phys. E **10**, 43 (2001).
[57] W. Grein, Nucl. Phys. B **131**, 255 (1977).
[58] V. Comparat, R. Frascaria, N. Marty, M. Morlet, and A. Willis, Nucl. Phys. A **221**, 403 (1974).
[59] P. G. Roos and N. S. Wall, Phys. Rev. **140**, B1237 (1965).
[60] V. V. Zerkin and B. Pritychenko, Nucl. Instrum. Methods Phys. Res. A **888**, 31 (2018).
[61] A. Ong, J. C. Berengut, and V. V. Flambaum, Phys. Rev. C **82**, 014320 (2010).
[62] I. Angeli and K. P. Marinova, At. Data Nucl. Data Tables **99**, 69 (2013).
[63] A. Trzcińska, J. Jastrzębski, P. Lubiński, F. J. Hartmann, R. Schmidt, T. von Egidy, and B. Kłos, Phys. Rev. Lett. **87**, 082501 (2001).
[64] M. Dutra, O. Lourenço, J. S. Sá Martins, A. Delfino, J. R. Stone, and P. D. Stevenson, Phys. Rev. C **85**, 035201 (2012).
[65] P. Sarriguren, M. K. Gaidarov, E. M. de Guerra, and A. N. Antonov, Phys. Rev. C **76**, 044322 (2007).
[66] S. Shen, H. Liang, W. H. Long, J. Meng, and P. Ring, Prog. Part. Nucl. Phys. **109**, 103713 (2019).
[67] M. Beiner, H. Flocard, N. Van Giai, and P. Quentin, Nucl. Phys. A **238**, 29 (1975).
[68] S. Hilaire and M. Girod, Eur. Phys. J. A **33**, 237 (2007);
[69] N. Van Giai and H. Sagawa, Phys. Lett. B **106**, 379 (1981).
[70] E. Chabanat, P. Bonche, P. Haensel, J. Meyer, and R. Schaeffer, Nucl. Phys. A **635**, 231 (1998).
[71] G. A. Lalazissis, T. Nikšić, D. Vretenar, and P. Ring, Phys. Rev. C **71**, 024312 (2005).
[72] S. Typel and H. H. Wolter, Nucl. Phys. A **656**, 331 (1999).
[73] T. Nikšić, D. Vretenar, and P. Ring, Phys. Rev. C **78**, 034318 (2008).
[74] W. H. Long, H. Sagawa, J. Meng, and N. Van Giai, Europhys. Lett. **82**, 12001 (2008).
[75] W. Long, J. Meng, N. Van Giai, and S.-G. Zhou, Phys. Rev. C **69**, 034319 (2004).
[76] W. H. Long, N. Van Giai, and J. Meng, Phys. Lett. B **640**, 150 (2006).
[77] Y. Sugahara and H. Toki, Nucl. Phys. A **579**, 557 (1994).
[78] P. W. Zhao, Z. P. Li, J. M. Yao, and J. Meng, Phys. Rev. C **82**, 054319 (2010).
[79] P.-G. Reinhard, M. Rufa, J. Maruhn, W. Greiner, and J. Friedrich, Z. Phys. A **323**, 13 (1986).
[80] G. A. Lalazissis, J. König, and P. Ring, Phys. Rev. C **55**, 540 (1997).
[81] M. Bender, K. Rutz, P.-G. Reinhard, J. A. Maruhn, and W. Greiner, Phys. Rev. C **60**, 034304 (1999).
[82] S. J. Lee, J. Fink, A. B. Balantekin, M. R. Strayer, A. S. Umar, P.-G. Reinhard, J. A. Maruhn, and W. Greiner, Phys. Rev. Lett. **57**, 2916 (1986).
[83] M. Honma, T. Otsuka, T. Mizusaki, and M. Hjorth-Jensen, Phys. Rev. C **80**, 064323 (2009).
[84] L. Xayavong and N. A. Smirnova, Phys. Rev. C **97**, 024324 (2018).
[85] A. Kohama, K. Iida, and K. Oyamatsu, Phys. Rev. C **78**, 061601(R) (2008).
[86] W. Horiuchi, T. Inakura, T. Nakatsukasa, and Y. Suzuki, Phys. Rev. C **86**, 024614 (2012).
[87] W. Horiuchi, T. Inakura, and S. Michimasa, Phys. Rev. C **105**, 014316 (2022).
[88] M. V. Stoitsov, N. Schunck, M. Kortelainen, N. Michel, H. Nam, E. Olsen, J. Sarich, and S. Wild, Comput. Phys. Commun. **184**, 1592 (2013).
[89] J. Bartel, P. Quentin, M. Brack, C. Guet, and H. Håkansson, Nucl. Phys. A **386**, 79 (1982).